Acta Crystallographica Section F
Structural Biology and Crystallization Communications
ISSN 1744-3091

X-ray structure of the SH3 domain of the phosphoinositide 3-kinase p85β subunit

Shuai Chen,[a]‡ Yibei Xiao,[a,b]‡ Rajesh Ponnusamy,[a]§ Jinzhi Tan,[a] Jian Lei[a] and Rolf Hilgenfeld[a,c,d]*

[a]Institute of Biochemistry, Center for Structural and Cell Biology in Medicine, University of Lübeck, Ratzeburger Allee 160, 23538 Lübeck, Germany, [b]Graduate School for Computing in Medicine and Life Sciences, University of Lübeck, Ratzeburger Allee 160, 23538 Lübeck, Germany, [c]Laboratory for Structural Biology of Infection and Inflammation, c/o DESY, Building 22a, Notkestrasse 85, 22603 Hamburg, Germany, and [d]Shanghai Institute of Materia Medica, Chinese Academy of Sciences, 555 Zu Chong Zhi Road, Shanghai 201203, People's Republic of China

‡ These authors contributed equally to this work.
§ Present address: Department of Medical Biochemistry and Biophysics, Karolinska Institutet, 17 177 Stockholm, Sweden.

Correspondence e-mail: hilgenfeld@biochem.uni-luebeck.de

Received 5 June 2011
Accepted 5 August 2011

PDB Reference: p85β SH3, 3o5z.

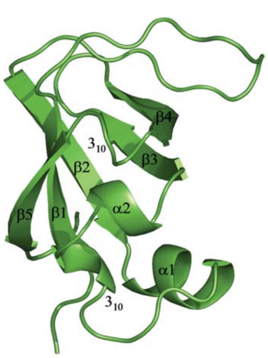

Src-homology 3 (SH3) domains are involved in extensive protein–protein interactions and constitute key elements of intracellular signal transduction. Three-dimensional structures have been reported for SH3 domains of various proteins, including the 85 kDa regulatory subunit (p85) of phosphoinositide 3-kinase. However, all of the latter structures are of p85 isoform α and no crystal structure of the SH3 domain of the equally important isoform β has been reported to date. In this structural communication, the recombinant production, crystallization and X-ray structure determination at 2.0 Å resolution of the SH3 domain of human p85β is described. The structure reveals a compact β-barrel fold very similar to that of p85α. However, binding studies with two classes of proline-rich ligand peptides demonstrate that the ligand-binding specificity differs slightly between the SH3 domains of human p85β and p85α, despite their high structural similarity.

1. Introduction

Being small intracellular protein modules composed of approximately 60 residues, Src-homology 3 (SH3) domains are abundant in signalling and cytoskeletal proteins (Koch *et al.*, 1991; Pawson & Gish, 1992). SH3 domains generally mediate protein–protein interactions through binding to proline-rich motifs in the target proteins and assemble multimeric signalling complexes to transduce intracellular signals (Rickles *et al.*, 1994).

Structure determination of SH3 domains has been the subject of much interest (Booker *et al.*, 1993; Kohda *et al.*, 1993; Koyama *et al.*, 1993; Noble *et al.*, 1993; Feng *et al.*, 1994; Lim *et al.*, 1994), as are functional studies of the proteins that contain them. An example is phosphoinositide 3-kinase (PI3K), which is a heterodimeric protein/lipid kinase with different isoforms. PI3K consists of a 110 kDa catalytic subunit (p110) that contains the kinase domain and an 85 kDa regulatory subunit (p85) that consists of two Src-homology 2 (SH2) domains and one SH3 domain (Inukai *et al.*, 2001). Besides regulating many important cellular processes such as proliferation, differentiation, apoptosis and vesicle transport (Cantley, 2002), PI3K is also known to become activated after influenza A virus infection; this is caused by the interaction of its p85 subunit with the viral nonstructural protein NS1, thereby inhibiting virus-induced cell death (Ehrhardt *et al.*, 2007). The p85 subunit can interact with phosphotyrosine residues on receptor proteins through one or both of its SH2 domains. Less information is known regarding the role of the p85 SH3 domain, although various proteins, including the influenza virus NS1 protein, have been identified to associate with it (Shin, Liu *et al.*, 2007; Shin, Li *et al.*, 2007). Both X-ray and NMR structures of the p85 SH3 domain have been determined previously (Booker *et al.*, 1993; Koyama *et al.*, 1993; Liang *et al.*, 1996). However, all of these structures are of isoform α of p85 and no X-ray structure of an SH3 domain from the equally important isoform β has been deposited in the PDB. Here, we fill this gap by reporting the crystal structure of the SH3 domain from human PI3K p85β at 2.0 Å resolution. Structural comparison of this protein with the human p85α SH3 domain and analysis of p85β SH3 binding to two proline-rich ligand peptides are also described in order to shed light on possible differences in ligand binding by these domains.

2. Experimental

The SH3 domain (residues 1–85) was amplified by PCR from an existing clone for full-length p85β of human PI3K with primers GGAAGGATCCATGGCGGCCCTGAGGGCTTC (forward) and CGCTCGAGTCACCGGGCCAGGGCCACGGG (reverse). The product was inserted between *Bam*HI and *Xho*I sites of the pGEX-6P-1 vector and the resulting plasmid was transformed into *Escherichia coli* BL21 (DE3) cells. Cultures were grown at 310 K to an OD_{600} of 0.6–0.8, which was followed by introducing IPTG to 1 m*M*; the N-terminal GST-fusion protein was produced at 298 K for 6 h. Freeze–thawed cell pellets were resuspended in lysis buffer (50 m*M* Tris–HCl pH 7.5, 500 m*M* NaCl, 5 m*M* DTT) supplemented with EDTA-free protease-cocktail inhibitor (Roche) and disrupted on ice by sonication. The crude lysate was centrifuged and the supernatant was filtered through a 0.45 µm filter (Sarstedt) followed by loading onto a 5 ml GSTrap FF column (GE Healthcare). The column was washed with lysis buffer and PreScission Cleavage Buffer (50 m*M* Tris–HCl pH 7.5, 150 m*M* NaCl, 1 m*M* EDTA and 1 m*M* DTT), followed by loading PreScission protease (GE Healthcare) onto the column. Cleavage was performed at 277 K overnight and the eluate samples containing the p85β SH3 domain were collected. The multimeric state of the p85β SH3 domain in solution was analyzed using size-exclusion chromatography (SEC) on a HiLoad 16/60 Superdex 75 column (GE Healthcare).

The binding affinities of two proline-rich ligand peptides to the p85β SH3 domain were measured using the surface plasmon resonance (SPR) method with a BIAcore 3000 instrument (GE Healthcare). The SH3 protein was immobilized on a CM5 biosensor chip and the binding curves of peptides I or II at various concentrations were recorded at 298 K. Dissociation constants (K_d) were calculated with the *BIAcore Analysis Software* by fitting the binding curves to a simple 1:1 ligand–receptor binding model.

The purified human p85β SH3 domain (in 10 m*M* Tris–HCl pH 7.5, 100 m*M* NaCl, 5 m*M* DTT) was concentrated to 15 mg ml^{-1} and crystallized by the sitting-drop vapour-diffusion method at 285 K using a Phoenix robot (Dunn Labortechnik). Initial hits were subsequently optimized by manually setting up 4 µl drops consisting of 2 µl protein solution and 2 µl reservoir solution. Optimum cube-like single crystals were obtained from 100 m*M* sodium cacodylate pH 6.0, 50 m*M* calcium acetate, 30% MPD. A crystal in the crystallization solution was directly flash-cooled in liquid nitrogen, as 30% MPD alone was a sufficient cryoprotectant. Diffraction data were collected at 100 K using synchrotron radiation (λ = 0.8123 Å) at the University of Hamburg–University of Lübeck–EMBL beamline X13 at DESY (Hamburg, Germany). The crystal diffracted to ~2.0 Å resolution and diffraction data were processed with *MOSFLM* (Leslie, 1992), followed by reduction and scaling with *SCALA* (Winn *et al.*, 2011; Evans, 1997). Molecular replacement was carried out with *Phaser* (McCoy *et al.*, 2007) using the SH3 domain of human p85α (PDB entry 1pht; Liang *et al.*, 1996) as a search model. *Coot* (Emsley & Cowtan, 2004) and *REFMAC*5 (Murshudov *et al.*, 2011) were subsequently employed for iterative cycles of model building and refinement. In the final steps of refinement, TLS restraints were incorporated (Painter & Merritt, 2006). Water molecules were identified with *Coot* based on the $F_o - F_c$ difference map. The superimposition of different structural models of SH3 domains was performed using the EBI *PDBeFold* web server (http://www.ebi.ac.uk/msd-srv/ssm/; Krissinel & Henrick, 2004). The stereochemical quality of the final model was validated by *PROCHECK* (Laskowski *et al.*, 1993). All figures were created using *PyMOL* (DeLano, 2002). Data-collection and refinement statistics are presented in Table 1.

Table 1
Data-collection and refinement statistics.

Values in parentheses are for the highest resolution shell.

Data-collection statistics	
Wavelength (Å)	0.8123
Space group	$P2_12_12_1$
Molecules per asymmetric unit	2
Unit-cell parameters	
a (Å)	46.01
b (Å)	57.79
c (Å)	62.97
Resolution range (Å)	21.37–2.01 (2.12–2.01)
Observed reflections	82380 (11925)
Unique reflections	11641 (1665)
Data multiplicity	7.1 (7.2)
Completeness (%)	99.9 (100)
$\langle I/\sigma(I)\rangle$	20.3 (3.8)
R_{merge}† (%)	4.9 (53.5)
V_M (Å^3 Da^{-1})	2.13
Solvent content (%)	42.34
Refinement statistics	
R_{work}‡	0.212
R_{free}‡	0.259
Total No. of atoms	1283
No. of residues	160
Chain *A*	3–84
Chain *B*	5–82
No. of water molecules	23
Average *B* factor of all atoms (Å^2)	
Protein main chains	51.27
Protein side chains	56.32
R.m.s.d. bond lengths§ (Å)	0.022
R.m.s.d. bond angles§ (°)	1.884
Ramachandran plot (%)	
Most favoured	97.4
Additional allowed	2.6
Outliers	0.0

† $R_{merge} = \sum_{hkl}\sum_i |I_i(hkl) - \langle I(hkl)\rangle| / \sum_{hkl}\sum_i I_i(hkl)$, where $I_i(hkl)$ and $\langle I(hkl)\rangle$ are the *i*th and the mean measurements of the intensity of unique reflection *hkl*, respectively. ‡ $R_{work} = \sum_{hkl} ||F_{obs}| - |F_{calc}|| / \sum_{hkl} |F_{obs}|$, where F_{obs} and F_{calc} are the observed and calculated structure-factor amplitudes, respectively, and the summation is over 95% of the reflections in the specified resolution range. The remaining 5% of the reflections were randomly selected before the structure refinement and were not included in the structure refinement. R_{free} is calculated over these reflections using the same equation as for R_{work}. § Root-mean-square deviations from the parameter set for ideal stereochemistry.

3. Results and discussion

The crystal of the human p85β SH3 domain (residues 1–85) belonged to the orthorhombic space group $P2_12_12_1$, with unit-cell parameters *a* = 46.01, *b* = 57.79, *c* = 62.97 Å. There were two molecules per asymmetric unit, giving a V_M value of 2.13 Å^3 Da^{-1}. The structure was determined at 2.0 Å resolution and electron density corresponding to residues 3–84 was well defined. A Ramachandran plot of the final model indicates that 97.4% of the residues are in the most favoured regions and 2.6% in additional allowed regions. As depicted in Fig. 1(*a*), the p85β SH3 domain features the typical antiparallel SH3 β-barrel built from two orthogonal β-sheets consisting of five antiparallel strands (β1–β5) and four loops containing two α-helices (α1–α2) and two short 3_{10}-helices. As described in previous publications (Booker *et al.*, 1993; Yu *et al.*, 1994), the long 'RT loop' (Arg- and Thr-containing loop; Musacchio, 2002) between strands β1 and β2 plays a key role in the function of the SH3 domain since numerous residues which are important for the binding of proline-rich peptide ligands are located in this loop (Fig. 1*b*). The residues of the SH3 domain involved in ligand binding are highly conserved between human p85α and p85β (Fig. 1*c*). In addition, the second loop connecting strands β2 and β3 of the SH3 domain from both p85α and p85β contains a unique insertion of 15 amino-acid residues, the longest insertion among all characterized SH3 domains (Koyama *et al.*, 1993). A structural comparison of the p85β SH3 domain (chain *A*)

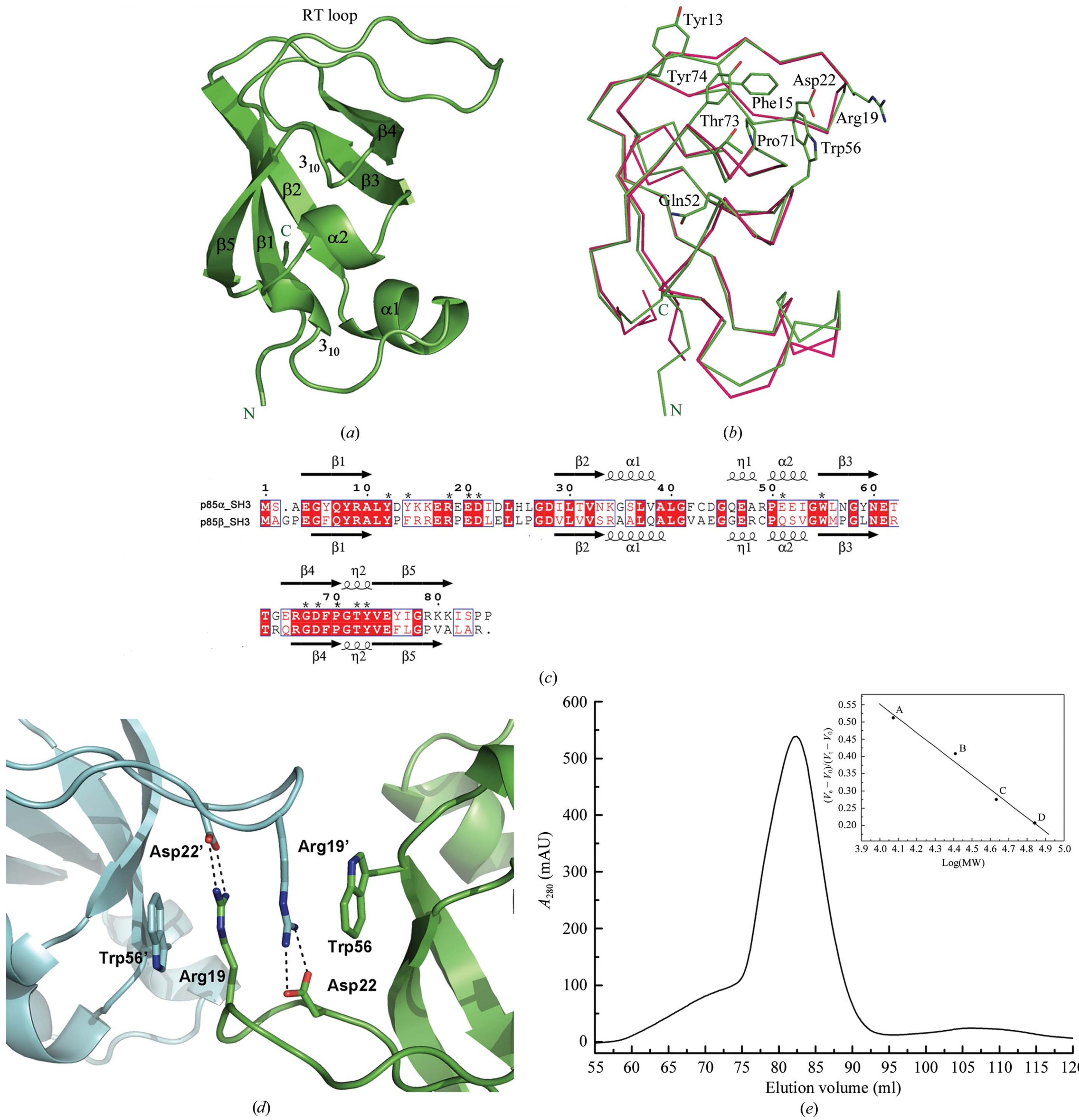

Figure 1

X-ray structure of the SH3 domain of the p85β subunit of human PI3K. (*a*) Ribbon drawing of the p85β SH3 domain. The N- and C-termini are labelled by the letters N and C, respectively. The α-helices (α1, 35–41; α2, 51–54), β-strands (β1, 6–11; β2, 28–34; β3, 56–61; β4, 65–71; β5, 75–81) and 3_{10}-helices (47–49 and 72–74) are labelled. (*b*) Superimposition of the SH3 domains of human p85β (chain *A*) and p85α (PDB entry 1pht; Liang *et al.*, 1996). The C^{α} trace of p85β SH3 is shown in green and that of p85α SH3 is shown in magenta. The conserved residues involved in ligand binding are highlighted by presentation in stick mode. (*c*) Structure-based sequence alignment of the p85α and p85β SH3 domains. The sequence alignment was performed with *ClustalW2* and the figure was generated using *ESPript* (Gouet *et al.*, 1999). Secondary structures of SH3 domains are indicated above and below the corresponding sequences. Residue numbers for the p85α SH3 domain (above) are also indicated and the residues involved in ligand binding are labelled with asterisks. (*d*) The interface of the noncrystallographic dimer of the p85β SH3 domain observed in the asymmetric unit. Ribbon structures of molecules *A* and *B* are coloured green and cyan, respectively. Residues Arg19 and Trp56 of molecule *A* stack with the same residues (indicated by primes) from the neighbouring molecule *B*. The salt bridges between Arg19 and Asp22′ and betweem Arg19′ and Asp22 are indicated by dotted lines. (*e*) SEC analysis of the p85β SH3 domain at a concentration of 5 mg ml^{-1}. The inset shows the calibrated gel-filtration data with four molecular-weight marker proteins.

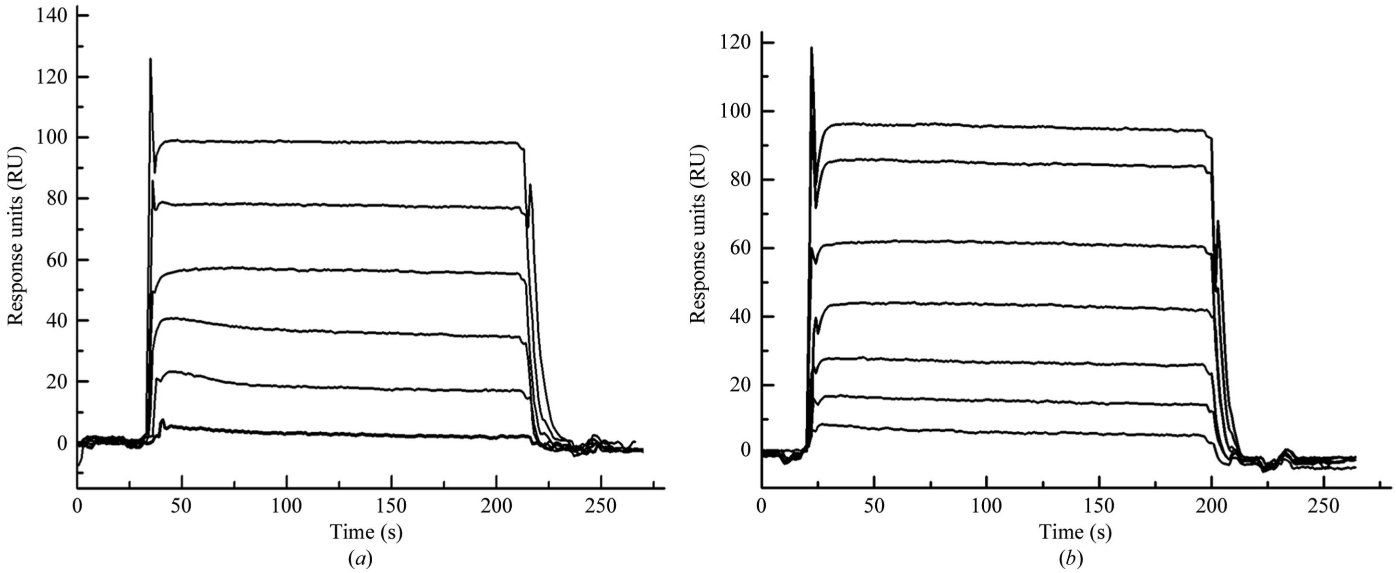

Position	P_{-6}	P_{-5}	P_{-4}	P_{-3}	P_{-2}	P_{-1}	P_0	P_1	P_2	P_3	P_4	P_5
Peptide used by Batra-Safferling *et al.* (2010)	H	S	K	R	P	L	P	P	L	P	S	L
Class I peptide used in the current study				R	K	L	P	P	R	P	S	K
	1	2	3	4	5	6	7	8	9	10	11	12

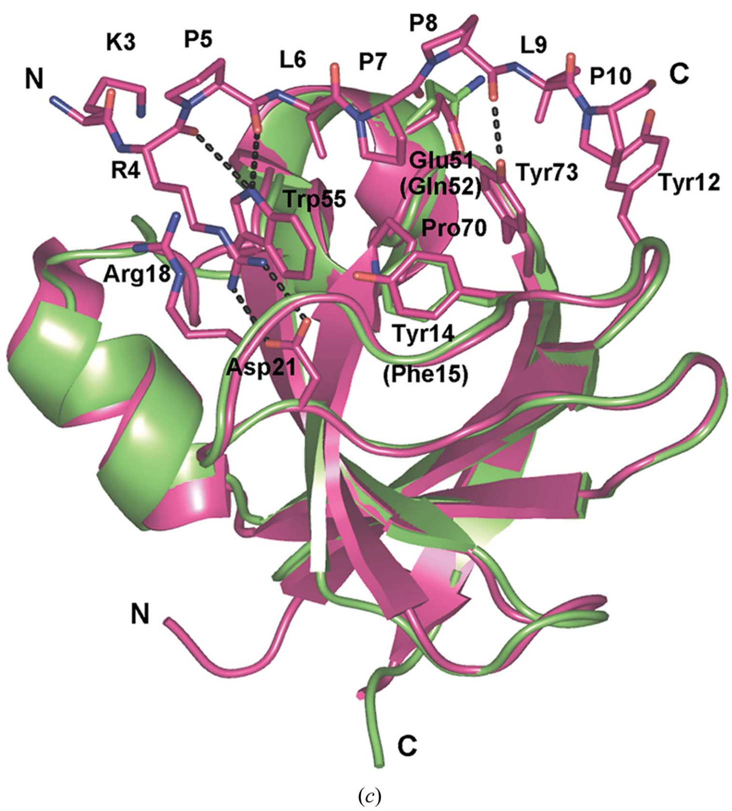

Figure 2
Binding of proline-rich ligand peptides to the human p85β SH3 domain. Real-time binding-affinity measurements of class I (RKLPPRPSK) (*a*) and class II (LNKPPLPKR) (*b*) ligand peptides to the p85β SH3 domain were obtained using the SPR method. Representative sensorgrams were obtained from injections of the peptides at concentrations varying from 1 to 500 μM (curves from bottom to top). The peptides were injected for 180 s and dissociation was monitored for more than 60 s. (*c*) Structural comparison of the p85β SH3 domain (chain *A*, green) with the complex of the p85α SH3 domain and a class I peptide (PDB entry 3i5r, magenta; Batra-Safferling *et al.*, 2010). The sequences of the bound peptide used by Batra-Safferling and coworkers and the class I peptide used in the current study are displayed above the structural superimposition. The residues of the bound peptide and the side chains of residues in the p85α SH3 domain involved in ligand binding are shown as sticks (magenta) and the residue numbers are indicated. The salt bridges and hydrogen bonds between the p85α SH3 domain and the peptide are shown as dotted lines. The side chains of equivalent residues in the p85β SH3 domain that are not identical to those involved in ligand binding by p85α are also highlighted in stick mode (green) and the residue numbers are indicated in brackets (Phe15 is equivalent to Tyr14 and Gln52 is equivalent to Glu51, as indicated in Fig. 1*c*).

with the published structure of human p85α SH3 (PDB entry 1pht; Liang *et al.*, 1996) yielded a root-mean-square (r.m.s.) distance of 0.92 Å for all 80 equivalent C$^\alpha$ atoms (Fig. 1*b*), indicating high structural similarity between the SH3 domains of the two p85 isoforms of PI3K. The r.m.s. distance between the two molecules in the asymmetric unit of the p85β SH3 domain is 0.36 Å; the noncrystallographic dimer of the p85β SH3 domain found in the asymmetric unit has a small total buried surface area of ~660 Å^2 and the interface mainly involves residues Arg19, Asp22 and Trp56 from neighbouring molecules. As shown in Fig. 1(*d*), Arg19 and Trp56 of molecule *A* stack with the same residues of the neighbouring molecule *B*, leaving the side chains of the Arg residues sandwiched between the indole rings of the tryptophans. In addition, a salt bridge between Arg19 and Asp22′ is also formed at the interface. It is worth noting that the dimer seen here also appears in the crystal structure of the human p85α SH3 domain through crystallographic symmetry (Liang *et al.*, 1996). In order to determine the assembly state of the p85β SH3 domain in solution, SEC analysis was performed. As indicated in Fig. 1(*e*), the protein eluted in a single peak with a retention volume of 82.3 ml, corresponding to an estimated molecular mass (MW) of 11.4 kDa. This implies that the p85β SH3 domain exists as a monomer in solution and that the dimer in the crystal is likely to be formed owing to advantageous packing. Furthermore, we observed that molecule *B* was linked by a disulfide bond involving Cys50 to the symmetry-related molecule *A*′ (symmetry operation $-x + 1, y - 1/2, -z + 1/2$). We postulate that the formation of this disulfide bond may be initiated by depletion of DTT during crystallization, because no disulfide bond was formed in solution for the p85β SH3 domain, as revealed by both nonreducing SDS–PAGE and native PAGE analyses (data not shown).

In order to further characterize the differences in ligand-binding specificity between the SH3 domains of human p85 isoforms β and α, the binding of ligand peptides to the p85β SH3 domain was examined. Two proline-rich peptides which have been demonstrated to bind to the p85α SH3 domain (K_d = 9.1 and 13 µ*M*) through screening of a combinatorial peptide library (Chen *et al.*, 1993) were selected for SPR measurements. These two ligands bind to the p85α SH3 domain in opposite orientations: a type I orientation was found with the peptide RKLPPRPSK (class I) and a type II orientation with the peptide LNKPPLPKR (class II) (Feng *et al.*, 1994; Yu *et al.*, 1994). As demonstrated in Figs. 2(*a*) and 2(*b*), both these peptides resulted in a significant and dose-dependent increase in SPR response units and presented characteristic fast-binding and fast-dissociation curves, indicating a rapidly formed and relatively unstable SH3–peptide complex. The peptide concentration series were fitted to a steady-state binding model for the calculation of binding affinities and the K_d values were determined as 19 µ*M* for the class I ligand and 74 µ*M* for the class II ligand, suggesting a weaker binding of these peptides to p85β SH3 compared with p85α. The X-ray structure of the p85α SH3 domain in complex with a class I peptide (HSKRPLPPLPSL) has recently been reported (Batra-Safferling *et al.*, 2010). As shown in Fig. 2(*c*), the peptide forms a typical left-handed polyproline helix in the complex and is bound to the SH3 domain in the type I orientation. The side chains of residues Arg4, Pro7 and Pro10 of the bound peptide are all facing the SH3 protein, forming extensive interactions. Superimposition of the p85β SH3 domain (chain *A*) and the structure of this complex gave an r.m.s. distance of 0.75 Å for all 78 equivalent C$^\alpha$ atoms (Fig. 2*c*), which is in agreement with the published finding that the ligand-bound conformation of the SH3 domain is essentially identical to its unbound state (Yu *et al.*, 1994; Batra-Safferling *et al.*, 2010). However, it should be noted that Leu is present at position P$_2$ of this bound peptide, while Arg is in the corresponding position in the class I peptide used by us (Fig. 2*c*). A previous report revealed that Arg at the P$_2$ position can form a salt bridge with residue Glu51 of p85α SH3 and that the E51Q mutation leads to reduction of the binding affinity of the class I peptide for the SH3 domain (Yu *et al.*, 1994). Interestingly, the equivalent residue in the p85β SH3 domain is not Glu but Gln (Figs. 1*c* and 2*c*), which might explain the decreased binding affinity of p85β SH3 for the peptides. We have also tried to crystallize complexes of the p85β SH3 domain with the two ligand peptides. It turned out that only the free SH3 domain and not its complexes with these peptides could be crystallized, probably owing to the decreased binding affinity between the peptides and the p85β SH3 domain. Therefore, sequence modification of the ligand peptides to optimize their binding affinities is probably required in order to obtain crystals of the complexes.

In summary, in this communication we have presented the X-ray structure of the human p85β SH3 domain as well as the characterization of the binding of two peptide ligands of the p85α SH3 domain to its p85β counterpart. Consistent with the published results for other SH3 domains, the protein shows a well conserved structural fold, highlighting that the various SH3 domains possess pronounced structural similarity to fulfil their biological functions. This structure fills a major gap, as no crystal structure of the important p85β SH3 domain was previously available.

This project was supported by the International Consortium on Anti-Virals (ICAV) and the DFG Cluster of Excellence ‘Inflammation at Interfaces’ (EXC 306). RH is supported by a Chinese Academy of Sciences Visiting Professorship for Senior International Scientists (Grant No. 2010T1S6) and by the Fonds der Chemischen Industrie. We thank Professor Stephan Ludwig (University of Münster, Germany) for providing the plasmid of full-length human p85β.

References

Batra-Safferling, R., Granzin, J., Mödder, S., Hoffmann, S. & Willbold, D. (2010). *Biol. Chem.* **391**, 33–42.
Booker, G. W., Gout, I., Downing, A. K., Driscoll, P. C., Boyd, J., Waterfield, M. D. & Campbell, I. D. (1993). *Cell*, **73**, 813–822.
Cantley, L. C. (2002). *Science*, **296**, 1655–1657.
Chen, J. K., Lane, W. S., Brauer, A. W., Tanaka, A. & Schreiber, S. L. (1993). *J. Am. Chem. Soc.* **115**, 12591–12592.
DeLano, W. L. (2002). *PyMOL*. http://www.pymol.org.
Ehrhardt, C., Wolff, T., Pleschka, S., Planz, O., Beermann, W., Bode, J. G., Schmolke, M. & Ludwig, S. (2007). *J. Virol.* **81**, 3058–3067.
Emsley, P. & Cowtan, K. (2004). *Acta Cryst.* D**60**, 2126–2132.
Evans, P. (1997). *CCP4 Newsl.* **33**, 22–24.
Feng, S., Chen, J. K., Yu, H., Simon, J. A. & Schreiber, S. L. (1994). *Science*, **266**, 1241–1247.
Gouet, P., Courcelle, E., Stuart, D. I. & Métoz, F. (1999). *Bioinformatics*, **15**, 305–308.
Inukai, K., Funaki, M., Anai, M., Ogihara, T., Katagiri, H., Fukushima, Y., Sakoda, H., Onishi, Y., Ono, H., Fujishiro, M., Abe, M., Oka, Y., Kikuchi, M. & Asano, T. (2001). *FEBS Lett.* **490**, 32–38.
Koch, C. A., Anderson, D., Moran, M. F., Ellis, C. & Pawson, T. (1991). *Science*, **252**, 668–674.
Kohda, D., Hatanaka, H., Odaka, M., Mandiyan, V., Ullrich, A., Schlessinger, J. & Inagaki, F. (1993). *Cell*, **72**, 953–960.
Koyama, S., Yu, H., Dalgarno, D. C., Shin, T. B., Zydowsky, L. D. & Schreiber, S. L. (1993). *Cell*, **72**, 945–952.
Krissinel, E. & Henrick, K. (2004). *Acta Cryst.* D**60**, 2256–2268.
Laskowski, R. A., MacArthur, M. W., Moss, D. S. & Thornton, J. M. (1993). *J. Appl. Cryst.* **26**, 283–291.
Leslie, A. G. W. (1992). *Jnt CCP4/ESF–EACBM Newsl. Protein Crystallogr.* **26**.
Liang, J., Chen, J. K., Schreiber, S. T. & Clardy, J. (1996). *J. Mol. Biol.* **257**, 632–643.

Lim, W. A., Richards, F. M. & Fox, R. O. (1994). *Nature (London)*, **372**, 375–379.
McCoy, A. J., Grosse-Kunstleve, R. W., Adams, P. D., Winn, M. D., Storoni, L. C. & Read, R. J. (2007). *J. Appl. Cryst.* **40**, 658–674.
Murshudov, G. N., Skubák, P., Lebedev, A. A., Pannu, N. S., Steiner, R. A., Nicholls, R. A., Winn, M. D., Long, F. & Vagin, A. A. (2011). *Acta Cryst.* D**67**, 355–367.
Musacchio, A. (2002). *Adv. Protein Chem.* **61**, 211–268.
Noble, M. E., Musacchio, A., Saraste, M., Courtneidge, S. A. & Wierenga, R. K. (1993). *EMBO J.* **12**, 2617–2624.
Painter, J. & Merritt, E. A. (2006). *Acta Cryst.* D**62**, 439–450.
Pawson, T. & Gish, G. D. (1992). *Cell*, **71**, 359–362.
Rickles, R. J., Botfield, M. C., Weng, Z., Taylor, J. A., Green, O. M., Brugge, J. S. & Zoller, M. J. (1994). *EMBO J.* **13**, 5598–5604.
Shin, Y.-K., Li, Y., Liu, Q., Anderson, D. H., Babiuk, L. A. & Zhou, Y. (2007). *J. Virol.* **81**, 12730–12739.
Shin, Y.-K., Liu, Q., Tikoo, S. K., Babiuk, L. A. & Zhou, Y. (2007). *J. Gen. Virol.* **88**, 13–18.
Winn, M. D. *et al.* (2011). *Acta Cryst.* D**67**, 235–242.
Yu, H., Chen, J. K., Feng, S., Dalgarno, D. C., Brauer, A. W. & Schreiber, S. L. (1994). *Cell*, **76**, 933–945.